NAVAL POSTGRADUATE SCHOOL

MONTEREY, CALIFORNIA

THESIS

AN EXAMINATION OF HIGHER-ORDER TREATMENTS OF BOUNDARY CONDITIONS IN SPLIT-STEP FOURIER PARABOLIC EQUATION MODELS

by

Savas Erdim

June 2015

Thesis Advisor:	Kevin B. Smith
Second Reader:	Daphne Kapolka

THIS PAGE INTENTIONALLY LEFT BLANK

REPORT DOCUMENTATION PAGE

Form Approved OMB No. 0704-0188

1. AGENCY USE ONLY *(Leave blank)*	**2. REPORT DATE** June 2015	**3. REPORT TYPE AND DATES COVERED** Master's Thesis

4. TITLE AND SUBTITLE
AN EXAMINATION OF HIGHER-ORDER TREATMENTS OF BOUNDARY CONDITIONS IN SPLIT-STEP FOURIER PARABOLIC EQUATION MODELS

5. FUNDING NUMBERS

6. AUTHOR(S) Savas Erdim

7. PERFORMING ORGANIZATION NAME(S) AND ADDRESS(ES)
Naval Postgraduate School
Monterey, CA 93943-5000

8. PERFORMING ORGANIZATION REPORT NUMBER

9. SPONSORING /MONITORING AGENCY NAME(S) AND ADDRESS(ES)
N/A

10. SPONSORING/MONITORING AGENCY REPORT NUMBER

11. SUPPLEMENTARY NOTES The views expressed in this thesis are those of the author and do not reflect the official policy or position of the Department of Defense or the U.S. Government. IRB Protocol number ____N/A____.

12a. DISTRIBUTION / AVAILABILITY STATEMENT
Approved for public release; distribution is unlimited

12b. DISTRIBUTION CODE
A

13. ABSTRACT (maximum 200 words)

Parabolic equation models solved using the split-step Fourier (SSF) algorithm, such as the Monterey Miami Parabolic Equation model, are commonly used to predict underwater sound propagation in deep and shallow water environments. Previous studies have shown that the SSF algorithm is very accurate in shallow water when there is no density discontinuity between the water column and the sediment, but less effective in the presence of realistic density discontinuities due to phase errors that accumulate after a few kilometers. In this thesis, the standard density-smoothing approach and an alternative hybrid split-step/finite difference method are compared. The goal is to decrease the phase errors and increase the model's long-range accuracy. Different depth meshes and range step sizes are implemented in the algorithm to find the optimum results for both approaches. It is shown that the density-smoothing method provides better results with small range step sizes, while the hybrid method is more effective using longer range step sizes. However, the smoothing approach provides a more stable convergence of results, whereas the hybrid method solution is more sensitive to change in computational grid sizes. A more detailed examination of the density smoothing approach suggests good accuracy for a few kilometers, while the hybrid method provides improved agreement with a benchmark solution at longer ranges.

14. SUBJECT TERMS
parabolic equation, Monterey Miami Parabolic Equation, split-step Fourier algorithm, density smoothing approach, hybrid split-step/finite difference method, Couple07.

15. NUMBER OF PAGES
59

16. PRICE CODE

17. SECURITY CLASSIFICATION OF REPORT	**18. SECURITY CLASSIFICATION OF THIS PAGE**	**19. SECURITY CLASSIFICATION OF ABSTRACT**	**20. LIMITATION OF ABSTRACT**
Unclassified	Unclassified	Unclassified	UU

NSN 7540-01-280-5500

Standard Form 298 (Rev. 2-89)
Prescribed by ANSI Std. 239-18

THIS PAGE INTENTIONALLY LEFT BLANK

Approved for public release; distribution is unlimited

AN EXAMINATION OF HIGHER-ORDER TREATMENTS OF BOUNDARY CONDITIONS IN SPLIT-STEP FOURIER PARABOLIC EQUATION MODELS

Savas Erdim
Lieutenant Junior Grade, Turkish Navy
B.S., Turkish Naval Academy, 2010

Submitted in partial fulfillment of the
requirements for the degree of

MASTER OF SCIENCE IN ENGINEERING ACOUSTICS

from the

NAVAL POSTGRADUATE SCHOOL
June 2015

Author: Savas Erdim

Approved by: Kevin B. Smith
Thesis Advisor

Daphne Kapolka
Second Reader

Daphne Kapolka
Chair, Engineering Acoustics Academic Committee

THIS PAGE INTENTIONALLY LEFT BLANK

ABSTRACT

Parabolic equation models solved using the split-step Fourier (SSF) algorithm, such as the Monterey Miami Parabolic Equation model, are commonly used to predict underwater sound propagation in deep and shallow water environments. Previous studies have shown that the SSF algorithm is very accurate in shallow water when there is no density discontinuity between the water column and the sediment, but less effective in the presence of realistic density discontinuities due to phase errors that accumulate after a few kilometers. In this thesis, the standard density-smoothing approach and an alternative hybrid split-step/finite difference method are compared. The goal is to decrease the phase errors and increase the model's long-range accuracy. Different depth meshes and range step sizes are implemented in the algorithm to find the optimum results for both approaches. It is shown that the density-smoothing method provides better results with small range step sizes, while the hybrid method is more effective using longer range step sizes. However, the smoothing approach provides a more stable convergence of results, whereas the hybrid method solution is more sensitive to change in computational grid sizes. A more detailed examination of the density smoothing approach suggests good accuracy for a few kilometers, while the hybrid method provides improved agreement with a benchmark solution at longer ranges.

THIS PAGE INTENTIONALLY LEFT BLANK

TABLE OF CONTENTS

THIS PAGE INTENTIONALLY LEFT BLANK

LIST OF FIGURES

THIS PAGE INTENTIONALLY LEFT BLANK

LIST OF ACRONYMS AND ABBREVIATIONS

FE	finite element
FFT	fast Fourier transform
IFD	implicit finite-difference
MMPE	Monterey-Miami parabolic equation
PE	parabolic equation
SPE	standard parabolic equation
SSF	split-step Fourier
SSF/FD	split-step Fourier/finite difference
TL	transmission loss
WAPE	wide-angle parabolic equation

THIS PAGE INTENTIONALLY LEFT BLANK

ACKNOWLEDGMENTS

I would like to thank my advisor, Professor Kevin B. Smith, for his great guidance and patience during my thesis work.

To my beloved wife, Betul, and my dear daughter, Azra, for always believing in me, and for supporting me all the time.

I want to express my gratitude to the Turkish Naval Forces for giving me an opportunity to acquire a degree from a great school.

THIS PAGE INTENTIONALLY LEFT BLANK

I. INTRODUCTION

A. BACKGROUND

The study of the parabolic equation (PE) approximation to the elliptic Helmholtz wave equation dates back to mid-1940s, when Leontovich and Fock introduced the PE method to the problem of radio-wave propagation in the atmosphere. Since then, propagation modeling using the PE has been successfully applied to microwave waveguides, optics, laser-beam propagation, plasma physics, seismic propagation and underwater acoustics [1]. Tappert was the first to introduce the PE method for underwater acoustic propagation in 1974 [2], and the split-step Fourier (SSF) algorithm to solve the PE was developed by Hardin and Tappert in 1973 [3]. Since then, many articles have been published to improve PE propagation modeling in the ocean. According to a survey made in 1990, over a period of 15 years, more than 120 articles and technical reports related to PE developments in underwater acoustics had been published, as well as many more after that time [1].

The main advantage of the parabolic equation is modeling underwater sound propagation in the ocean at long-range and in range-dependent environments [4]. Several methods and algorithms have been introduced to solve the parabolic equation. The most common ones are the SSF algorithm, the implicit finite difference (IFD) algorithm, and the finite element (FE) method. There are many advantages and disadvantages to these techniques. For SSF, the primary advantage is its speed and simplicity [5]. Also, the SSF is efficient for long-range, narrow-angle propagation problems in range-dependent media. In environments causing strong bottom interactions, however, it loses some of its accuracy. IFD and FE methods give more accurate results in wide-angle, bottom-interacting, and range-independent media. However, they are generally less efficient and less stable than the SSF algorithm [1].

The standard parabolic approximation originally developed by Tappert was valid only for small angles, and its accuracy was degraded by the phase errors. Several attempts were made to reduce these errors and support wider angles of propagation.

Thompson and Chapman introduced the wide-angle parabolic equation (WAPE) approximation, which was based on Feit and Fleck's operator splitting [6]. This approach treats the square-root operator in a way that differs from the standard parabolic equation (SPE). It improved the parabolic equation by increasing the propagation angle from around 15 degrees to 40 degrees, reducing the phase errors while retaining the usage of the efficient SSF algorithm [4].

As previously stated, the SSF algorithm is known to be less accurate in the presence of strong bottom interactions. In order to treat the density contrasts at the interfaces between differing media (e.g., water and sediment), a general smoothing function is applied to the interface. This smoothing approach is the primary cause of the phase errors due to density discontinuity at the interface for long-range propagation. In 1996, Yevick and Thomson introduced a hybrid split-step/finite difference (SSF/FD) technique for modeling acoustic propagation in the presence of non-uniform density profiles [7]. This method offers a practical way to adapt existing SSF-based models by separating the operator approximations into density-dependent and density-independent components rather than relying on smoothing parameters. An overview of this method is presented in this thesis with specific numerical examples showing the improvements in the solutions.

B. PROBLEM STATEMENT

The Monterey-Miami Parabolic Equation (MMPE) model was developed in the mid-1990s and since then has been tested for several existing benchmark scenarios. The MMPE method computes the underwater acoustic propagation by using the SSF algorithm [8]. There are various versions of MMPE, including both 2D and 3D versions, versions that incorporate rough surfaces, oceanographic internal waves, and a variety of other environmental perturbations. In all cases, however, it applies the WAPE approximation of Thomson and Chapman [4].

Various techniques have been developed to treat the density discontinuity in the bottom interaction in order to increase the accuracy of MMPE. In this thesis, our goal is to compare the effects of Tappert's standard density smoothing approach and Yevick and

Thomson's hybrid split-step/finite difference algorithm [7] in the case of the bottom interactions for shallow water. We will perform the propagation in a simple Pekeris waveguide defined by Paul Hursky [9] and previously investigated by Owens [8] and Smith et al. [10].

In order to avoid any issues with implementation details in the existing MMPE model, a Matlab version of the SSF algorithm has been developed for this thesis based on the same operator approximations as the MMPE model. It was also written only for the simple, range-independent Pekeris waveguide that motivated this study.

THIS PAGE INTENTIONALLY LEFT BLANK

II. THEORY

A. PARABOLIC EQUATION DERIVATION

We start with the 2-D Helmholtz wave equation in cylindrical coordinates,

$$\frac{1}{r}\frac{\partial}{\partial r}\left(r\frac{\partial p}{\partial r}\right)+\rho\frac{\partial}{\partial z}\left(\frac{1}{\rho}\frac{\partial p}{\partial z}\right)+k_0^2 n^2 p=0, \tag{1}$$

where $k_0=\dfrac{\omega}{c_0}$ is the reference wave number, $n=\dfrac{c_0}{c(\mathrm{r},\mathrm{z})}$ is the acoustic index of refraction, c_0 is the reference sound speed, $c(\mathrm{r},\mathrm{z})$ is the spatially varying acoustic sound speed, and $\rho(z)$ is the density that is assumed to change only with depth. All features of the environment are presented in $c(\mathrm{r},\mathrm{z})$ and $\rho(\mathrm{z})$. We define the PE field function Ψ according to

$$\Psi(\mathrm{r},\mathrm{z})=\sqrt{k_0 r}\,p(\mathrm{r},\mathrm{z})\,\mathrm{e}^{-ik_0 r}, \tag{2}$$

which leads to the fundamental parabolic equation

$$\frac{\partial\Psi}{\partial r}=ik_0\left(Q-1\right)\Psi \tag{3}$$

where the square-root operator Q is defined as

$$Q=\sqrt{n^2+\frac{1}{k_0^2}\rho\frac{\partial}{\partial z}\left(\frac{1}{\rho}\frac{\partial}{\partial z}\right)}. \tag{4}$$

We can also define the field function as

$$\tilde{\Psi}=\sqrt{\rho}\Psi, \tag{5}$$

which satisfies the PE

$$\frac{\partial\tilde{\Psi}}{\partial r}=ik_0\left(\tilde{Q}-1\right)\tilde{\Psi}. \tag{6}$$

Here, the square-root operator takes the more compact form of

$$\tilde{Q} = \sqrt{\tilde{n}^2 + \frac{1}{k_0^2}\frac{\partial^2}{\partial z^2}}, \tag{7}$$

and the effective index of refraction, $\tilde{n}$, is defined as

$$\tilde{n}^2 = n^2 + \frac{1}{2k_0^2}\left[\frac{1}{\rho}\frac{\partial^2 \rho}{\partial z^2} - \frac{3}{2}\left(\frac{1}{\rho}\frac{\partial \rho}{\partial z}\right)^2\right]. \tag{8}$$

The original SSF algorithm is based on (8), which is discussed further in the section describing the smoothing approach. Either PE allows for a one-way marching algorithm solution of the form

$$\Psi(\mathrm{r}+\Delta \mathrm{r}, \mathrm{z}) = \exp\left[ik_0 \Delta \mathrm{r}(Q-1)\right]\Psi(\mathrm{r}, \mathrm{z}) \tag{9}$$

or similar for $\tilde{\Psi}$ and $\tilde{Q}$. We can define the operators as

$$\varepsilon = n^2 - 1, \;\; \mu = \frac{1}{k_0^2}\frac{\partial^2}{\partial z^2}, \text{ and } \gamma = -\frac{1}{k_0^2 \rho}\frac{\partial \rho}{\partial z}\frac{\partial}{\partial z}. \tag{10}$$

The original square root-operator then becomes

$$\begin{aligned} Q &= \sqrt{n^2 + \frac{1}{k_0^2}\rho\frac{\partial}{\partial z}\left(\frac{1}{\rho}\frac{\partial}{\partial z}\right)} \\ &= \sqrt{1 + \left(n^2 - 1\right)\frac{1}{k_0^2}\rho\left(-\frac{1}{\rho^2}\frac{\partial \rho}{\partial z}\frac{\partial}{\partial z} + \frac{1}{\rho}\frac{\partial^2}{\partial z^2}\right)}, \\ &= \sqrt{1 + (\mathrm{n}^2 - 1) + \frac{1}{k_0^2}\frac{\partial^2}{\partial z^2} - \frac{1}{k_0^2 \rho}\frac{\partial \rho}{\partial z}\frac{\partial}{\partial z}} \\ &= \sqrt{1 + \varepsilon + \mu + \gamma} \end{aligned} \tag{11}$$

which requires further approximation in order to implement the marching algorithm.

The MMPE model utilizes the Thomson-Chapman WAPE, defined by the operator splitting of Feit and Fleck [6],

$$Q_1' = \sqrt{1+\gamma} + \sqrt{1+\mu} + \sqrt{1+\varepsilon} - 2. \tag{12}$$

Then the propagator in the marching algorithm takes the form

$$\begin{aligned}\exp\left[ik_0\Delta r(Q'-1)\right] &= \exp\left[i\delta\left(\sqrt{1+\gamma}+\sqrt{1+\mu}+\sqrt{1+\varepsilon}-3\right)\right] \\ &\approx \exp\left[i\delta\left(\sqrt{1+\gamma}-1\right)\right]\exp\left[i\delta\left(\sqrt{1+\mu}-1\right)\right]\exp\left[i\delta\left(\sqrt{1+\varepsilon}-1\right)\right] \\ &= \exp\left[i\delta\left(\sqrt{1+\gamma}-1\right)\right]\exp\left[i\delta\left(\sqrt{1+\mu}-1\right)\right]\exp\left[i\delta\left(n-1\right)\right]\end{aligned} \tag{13}$$

where $\delta=k_0\Delta r$ and the non-commuting terms of the operators ε, μ, and γ are neglected in the second line. As strictly noted by Yevick and Thomson [7], the operation order in (13) is very important, and the γ term should be applied at the end of the range step, following application of the μ term.

The operator currently used in MMPE does not contain a γ term, since the density terms are built into the effective index of refraction. In this case, we simply define

$$\tilde{Q}_1 = \sqrt{1+\mu}+\sqrt{1+\tilde{\varepsilon}}-1\ , \tag{14}$$

where $\tilde{\varepsilon}=\tilde{n}^2-1$. The WAPE approximation does not consider the lowest order cross terms between operators, so the lowest order correction becomes

$$\begin{aligned}Q_2' &= Q_1' - \frac{1}{8}\left[\left(\varepsilon+\mu+\gamma\right)^2-\varepsilon^2-\mu^2-\gamma^2\right] \\ &= Q_1' - \frac{1}{8}\left[\varepsilon\left(\mu+\gamma\right)+\left(\mu+\gamma\right)\varepsilon+\mu\gamma+\gamma\mu\right].\end{aligned} \tag{15}$$

For completeness, note that the lowest order correction to the smoothing approach would be

$$\begin{aligned}\tilde{Q}_2 &= \tilde{Q}_1 - \frac{1}{8}\left[\left(\varepsilon+\mu\right)^2-\varepsilon^2-\mu^2\right] \\ &= \tilde{Q}_1 - \frac{1}{8}\left[\varepsilon\mu+\mu\varepsilon\right].\end{aligned} \tag{16}$$

In the SSF algorithm, ε and μ are just scalar operators in the physical (z) and wavenumber spaces (k_z), respectively.

If the γ terms and cross terms are added later as corrections, then we can define an intermediate step solution as

$$\tilde{\Psi}(\mathrm{r}+\Delta\mathrm{r},\mathrm{z}) = FFT^{-1}\left\{\exp\left[i\delta\left(\sqrt{1-\frac{k_z^2}{k_0^2}}-1\right)\right] x\, FFT\left[\exp\left(i\delta(\mathrm{n}-1)\right)\Psi(\mathrm{r},\mathrm{z})\right]\right\}, \quad (17)$$

where we have replaced $\sqrt{1+\mu} \Rightarrow \sqrt{1-\frac{k_z^2}{k_0^2}}$ and $\sqrt{1+\varepsilon} \Rightarrow n$, consistent with the application in the k_z-domain and z-domain. Note that the complete range step in the existing MMPE code is obtained by replacing $n \Rightarrow \tilde{n}$, where $\Psi(\mathrm{r},\mathrm{z})$ is replaced by $\tilde{\Psi}(\mathrm{r},\mathrm{z})$.

B. DENSITY-SMOOTHING APPROACH

The treatment of the density discontinuity in the MMPE model utilizes a density-smoothing approach at the water-bottom interface. As presented in (8), instead of the standard index of refraction, n, we define an effective index of refraction, $\tilde{n}$, by

$$\tilde{n}^2 = n^2 + \frac{1}{2k_0^2}\left[\frac{1}{\rho}\frac{\partial^2\rho}{\partial\mathrm{z}^2} - \frac{3}{2}\left(\frac{1}{\rho}\frac{\partial\rho}{\partial\mathrm{z}}\right)^2\right]. \quad (18)$$

The density discontinuity at the water-bottom interface can be defined as

$$\rho(\mathrm{z}) = \rho_w + (\rho_b - \rho_w)\,\bar{\mathrm{H}}(\mathrm{z}-\mathrm{z}_b), \quad (19)$$

where ρ_w and ρ_b are the water column and bottom sediment densities, respectively, and are assumed to be constants. The function $\bar{H}$ serves as an approximation to the Heaviside step function and defines a smooth transition according to

$$\bar{H}(\mathrm{z}-\mathrm{z}_b) = \bar{H}(\zeta) = \frac{1}{2}\left[1+\tanh(\frac{\zeta}{2L})\right], \quad (20)$$

where $\zeta = z\text{-}z_b$, and L defines the mixing length.

The first and second derivatives of the density are defined in the effective index of refraction as

$$\frac{\partial \rho}{\partial z} = (\rho_b - \rho_w)\frac{\partial \bar{H}}{\partial z} = \frac{(\rho_b - \rho_w)}{4L}\operatorname{sech}^2\left(\frac{\zeta}{2L}\right) \tag{21}$$

and

$$\frac{\partial^2 \rho}{\partial z^2} = (\rho_b - \rho_w)\frac{\partial^2 \bar{H}}{\partial z^2} = -\frac{(\rho_b - \rho_w)}{4L^2}\tanh\left(\frac{\zeta}{2L}\right)\operatorname{sech}^2\left(\frac{\zeta}{2L}\right). \tag{22}$$

These expressions are then implemented into (18) to define the effective index of refraction.

C. HYBRID SPLIT-STEP / FINITE DIFFERENCE IMPLEMENTATION TECHNIQUE

The hybrid split-step/finite difference PE algorithm for variable density media was introduced by Yevick and Thomson in 1996 [7]. Instead of relying on a smoothing function to transition the density discontinuity across the interface, they used a hybrid technique to specifically solve for the terms containing the density contrast. This approach can easily be implemented into existing SSF codes. To accomplish this, they separated the effects of the density by splitting the propagator into density-dependent and -independent components, as described in the previous section. In this approach, the density propagator is solved by using the finite difference technique and a Padè expansion [7].

The hybrid approach proposes that Q_1' requires an additional operation to (17), given by

$$\Psi'(\mathrm{r}+\Delta \mathrm{r}, \mathrm{z}) = \exp\left[i\delta\left(\sqrt{1+\gamma}-1\right)\right]\tilde{\Psi}(\mathrm{r}+\Delta \mathrm{r}, \mathrm{z}). \tag{23}$$

If we intend to invoke only the Q_1' approximation, then this completes the range step calculation, and $\Psi' \Rightarrow \Psi$. Here, the additional operation is approximated by a Padé expansion defined as

$$\exp\left[i\delta\left(\sqrt{1+\gamma}-1\right)\right] \approx \frac{1+\frac{1}{4}(1+i\delta)\gamma}{1+\frac{1}{4}(1-i\delta)\gamma}. \tag{24}$$

In order to employ a finite difference approach, we then write (23) as

$$\left[1+\frac{1}{4}(1-i\delta)\gamma\right]\Psi(\mathrm{r}+\Delta\mathrm{r},\mathrm{z}) = \left[1+\frac{1}{4}(1+i\delta)\gamma\right]\tilde{\Psi}(\mathrm{r}+\Delta\mathrm{r},\mathrm{z}). \tag{25}$$

Since direct application of γ is problematic, Yevick and Thomson proposed an alternative transverse operator:

$$\mu' = \frac{\rho}{k_0^2}\frac{\partial}{\partial \mathrm{z}}\left(\frac{1}{\rho}\frac{\partial}{\partial \mathrm{z}}\right). \tag{26}$$

Then $\gamma = \mu' - \mu,$ where both μ' and μ are well defined operators on Ψ.

1. Finite Difference Technique

Consider a discretely sampled environment and associated field where index $j=nb$ coincides with the water-bottom interface, $j<nb$ is in the water at the shallower depths and $j>nb$ is in the bottom at deeper depths.

$$\begin{aligned} \rho(\mathrm{j} < nb) &= \rho_w; \\ \rho(\mathrm{j} = nb) &= \frac{1}{2}(\rho_w + \rho_b); \\ \rho(\mathrm{j} > nb) &= \rho_b . \end{aligned} \tag{27}$$

The issue here is the evaluation of the term $\frac{\rho}{k_0^2}\frac{\partial}{\partial \mathrm{z}}\left(\frac{1}{\rho}\frac{\partial \Psi}{\partial \mathrm{z}}\right)$.

Assuming a smooth, continuous function, a 3-point centered difference scheme to evaluate the derivative is defined by

$$f_0' \simeq \frac{1}{2h}(\mathrm{f}_1 - \mathrm{f}_{-1}), \tag{28}$$

where $f_{\pm 1}$ is the function evaluated at the index ± 1, separated at a distance 2*h*, to give an approximation to the first derivative of the function at the midpoint index 0. Equivalently, if we sampled at half index values, then $f_0' \simeq \frac{1}{h}\left(f_{\frac{1}{2}} - f_{-\frac{1}{2}} \right)$.

When the term f_0' above is discretized and evaluated with this approximation, we obtain

$$\begin{aligned} \frac{\rho}{k_0^2}\frac{\partial}{\partial z}\left(\frac{1}{\rho}\frac{\partial \Psi}{\partial z}\right) &\simeq \frac{\rho}{k_0^2 \Delta z}\left[\frac{1}{\rho_{\frac{1}{2}}}\left(\frac{\partial \Psi}{\partial z}\right)_{\frac{1}{2}} - \frac{1}{\rho_{-\frac{1}{2}}}\left(\frac{\partial \Psi}{\partial z}\right)_{-\frac{1}{2}}\right] \\ &\simeq \frac{\rho}{k_0^2 (\Delta z)^2}\left[\frac{1}{\rho_{\frac{1}{2}}}\left(\Psi_1 - \Psi_0\right) - \frac{1}{\rho_{-\frac{1}{2}}}\left(\Psi_0 - \Psi_{-1}\right)\right]. \end{aligned} \tag{29}$$

In a previous analysis by Smith [11], implemented by Owens in 2014 [8], it was assumed that since ρ is discontinuous at the interface, then the factors $\rho \pm \frac{1}{2}$ could simply be replaced by their appropriate values above or below the index being evaluated. However, it has been determined that for the finite difference approximation to hold, ρ must be treated as a continuous function in the vicinity of index *j*. In this case, as was defined by Thomson [12],

$$\rho_{\frac{1}{2}} = \frac{1}{2}(\rho_1 + \rho_0)\,,\ \rho_{-\frac{1}{2}} = \frac{1}{2}(\rho_0 + \rho_{-1}). \tag{30}$$

2. Application of Finite Difference Approximations to Field Operators

Returning to our field operators μ and μ', we find

$$\begin{aligned} \mu \Psi = \frac{1}{k_0^2}\frac{\partial^2}{\partial z^2}\Psi = \frac{1}{k_0^2}\frac{\partial}{\partial z}\left(\frac{\partial \Psi}{\partial z}\right) &\approx \frac{1}{k_0^2 \Delta z}\left[\left(\frac{\partial \Psi}{\partial z}\right)_{\frac{1}{2}} - \left(\frac{\partial \Psi}{\partial z}\right)_{-\frac{1}{2}}\right] \\ \approx \frac{1}{\left(k_0 \Delta z\right)^2}\left[\left(\Psi_1 - \Psi_0\right) - \left(\Psi_0 - \Psi_{-1}\right)\right] &= \frac{1}{\left(k_0 \Delta z\right)^2}\left[\Psi_1 - 2\Psi_0 + \Psi_{-1}\right] \end{aligned} \tag{31}$$

and

$$\mu'\Psi = \frac{\rho}{k_0^2}\frac{\partial}{\partial z}\left(\frac{1}{\rho}\frac{\partial \Psi}{\partial z}\right) \approx \frac{\rho_0}{k_0^2(\Delta z)^2}\left[\frac{1}{\rho_{\frac{1}{2}}}\left(\Psi_1 - \Psi_0\right) - \frac{1}{\rho_{-\frac{1}{2}}}\left(\Psi_0 - \Psi_{-1}\right)\right]$$
$$= \frac{\rho_0}{\left(k_0 \Delta z\right)^2}\left[\frac{1}{\rho_{\frac{1}{2}}}\Psi_1 - \left(\frac{1}{\rho_{\frac{1}{2}}} + \frac{1}{\rho_{-\frac{1}{2}}}\right)\Psi_0 + \frac{1}{\rho_{-\frac{1}{2}}}\Psi_{-1}\right]. \tag{32}$$

Combining (31) and (32) with $\gamma = \mu' - \mu$, we obtain

$$\gamma\Psi = (\mu' - \mu)\Psi \approx \frac{1}{\left(k_0 \Delta z\right)^2}\left[\left(\frac{\rho_0}{\rho_{\frac{1}{2}}} - 1\right)\Psi_1 - \left(\frac{\rho_0}{\rho_{\frac{1}{2}}} + \frac{\rho_0}{\rho_{-\frac{1}{2}}} - 2\right)\Psi_0 + \left(\frac{\rho_0}{\rho_{-\frac{1}{2}}} - 1\right)\Psi_{-1}\right]$$
$$= \frac{1}{\left(k_0 \Delta z\right)^2}\left[\left(\rho_+ - 1\right)\Psi_1 - \left(\tilde{\rho} - 2\right)\Psi_0 + \left(\rho_- - 1\right)\Psi_{-1}\right] \tag{33}$$

where

$$\rho_+ \equiv \frac{\rho_0}{\rho_{\frac{1}{2}}} = \frac{\rho_0}{\frac{1}{2}\left(\rho_1 + \rho_0\right)},$$
$$\rho_- \equiv \frac{\rho_0}{\rho_{-\frac{1}{2}}} = \frac{\rho_0}{\frac{1}{2}\left(\rho_0 + \rho_{-1}\right)}, \tag{34}$$
$$\tilde{\rho} \equiv \rho_+ + \rho_- = \frac{\rho_0}{\rho_{\frac{1}{2}}} + \frac{\rho_0}{\rho_{-\frac{1}{2}}} = 2\rho_0\left[\frac{1}{\left(\rho_1 + \rho_0\right)} + \frac{1}{\left(\rho_0 + \rho_{-1}\right)}\right].$$

Here, the definition of $\tilde{\rho}$ matches the definition of the variable ρ_0 in Yevick and Thomson's paper. However, we reserve ρ_0 to designate the values of density at the central index *j=0*.

In order to find the solution, we can solve the tridiagonal matrix expression

$$\underline{A}\vec{\Psi} = \underline{B}\vec{\tilde{\Psi}}\,, \tag{35}$$

where $\underline{A} = \left[1 + \frac{1}{4}(1 - i\delta)\gamma\right]$ and $\underline{B} = \left[1 + \frac{1}{4}(1 + i\delta)\gamma\right]$. $\underline{A}$ and $\underline{B}$ are just identity matrices except in the vicinity of $z \sim z_b$, where γ is not zero. Note that the field vectors Ψ and $\tilde{\Psi}$ in (25) are now explicitly written as vectors over depth, $\vec{\Psi}$ and $\vec{\tilde{\Psi}}$. The solution of (35) completes the range step by applying the density operator term in the Q_1' operator.

3. Higher Order Correction Implementation

Yevick and Thomson [7] also proposed a higher order correction term in Q_2' given by

$$\exp\left\{-\frac{i\delta}{8}\left[\varepsilon(\mu+\gamma)+(\mu+\gamma)\varepsilon+\mu\gamma+\gamma\mu\right]\right\}. \tag{36}$$

Since $\mu + \gamma = \mu'$, this may be approximated by

$$\exp\left\{-\frac{i\delta}{8}\left[\varepsilon\mu'+\mu'\varepsilon+\mu\gamma+\gamma\mu\right]\right\} \simeq \frac{1-\frac{1}{16}i\delta\left(\varepsilon\mu'+\mu'\varepsilon+\mu\gamma+\gamma\mu\right)}{1+\frac{1}{16}i\delta\left(\varepsilon\mu'+\mu'\varepsilon+\mu\gamma+\gamma\mu\right)}. \tag{37}$$

Note that if $\gamma = 0$, then this higher order correction becomes simply

$$\exp\left[-\frac{i\delta}{8}\left(\varepsilon\mu+\mu\varepsilon\right)\right] \approx \frac{1-\frac{1}{16}i\delta\left(\varepsilon\mu+\mu\varepsilon\right)}{1+\frac{1}{16}i\delta\left(\varepsilon\mu+\mu\varepsilon\right)}. \tag{38}$$

This term can be applied to the existing MMPE approach based on the operator approximation $\tilde{Q}_2$.

Yevick and Thomson dropped the $\mu\gamma$ and $\gamma\mu$ terms since these give third-order derivatives and only the lowest order terms are used in the finite difference approximation. Instead, they utilized the correction as

$$\exp\left[-\frac{i\delta}{8}\left(\varepsilon\mu'+\mu'\varepsilon\right)\right]\approx\frac{1-\frac{1}{16}i\delta\left(\varepsilon\mu'+\mu'\varepsilon\right)}{1+\frac{1}{16}i\delta\left(\varepsilon\mu'+\mu'\varepsilon\right)}. \tag{39}$$

This produces the additional correction

$$\Psi(\mathrm{r}+\Delta\mathrm{r},\mathrm{z})=\exp\left[-\frac{i\delta}{8}\left(\varepsilon\mu'+\mu'\varepsilon\right)\right]\Psi'(\mathrm{r}+\Delta\mathrm{r},\mathrm{z}), \tag{40}$$

where we again invoke the matrix approach

$$\underline{A}\bar{\Psi}=\underline{B}\bar{\Psi}'. \tag{41}$$

The elements of the matrix $\underline{A}$ and $\underline{B}$ are defined by $\underline{A}=\left[1+\frac{i\delta}{16}\left(\varepsilon\mu'+\mu'\varepsilon\right)\right]$ and $\underline{B}=\left[1-\frac{i\delta}{16}\left(\varepsilon\mu'+\mu'\varepsilon\right)\right]$. Here, $\varepsilon\mu'\Psi$ follows (32) as,

$$\begin{aligned}\varepsilon\mu'\Psi&=\frac{\varepsilon_0\rho_0}{\left(k_0\Delta\mathrm{z}\right)^2}\left[\frac{1}{\rho_{\frac{1}{2}}}\Psi_1-\left(\frac{1}{\rho_{\frac{1}{2}}}+\frac{1}{\rho_{-\frac{1}{2}}}\right)\Psi_0+\frac{1}{\rho_{-\frac{1}{2}}}\Psi_{-1}\right]\\&=\frac{\varepsilon_0}{\left(k_0\Delta\mathrm{z}\right)^2}\left[\rho_+\Psi_1-\tilde{\rho}\Psi_0+\rho_-\Psi_{-1}\right]\end{aligned} \tag{42}$$

and $\mu'(\varepsilon\Psi)$ becomes

$$\begin{aligned}\mu'(\varepsilon\Psi)&=\frac{\rho_0}{k_0^2}\frac{\partial}{\partial\mathrm{z}}\left[\frac{1}{\rho}\frac{\partial(\varepsilon\Psi)}{\partial\mathrm{z}}\right]\simeq\frac{\rho_0}{k_0^2\Delta\mathrm{z}}\frac{\partial}{\partial\mathrm{z}}\left[\frac{1}{\rho}\left(\varepsilon_{\frac{1}{2}}\Psi_{\frac{1}{2}}-\varepsilon_{-\frac{1}{2}}\Psi_{-\frac{1}{2}}\right)\right]\\&=\frac{\rho_0}{\left(k_0\Delta\mathrm{z}\right)^2}\left[\frac{1}{\rho_{\frac{1}{2}}}\left(\varepsilon_1\Psi_1-\varepsilon_0\Psi_0\right)-\frac{1}{\rho_{-\frac{1}{2}}}\left(\varepsilon_0\Psi_0-\varepsilon_{-1}\Psi_{-1}\right)\right]\\&=\frac{\rho_0}{\left(k_0\Delta\mathrm{z}\right)^2}\left[\frac{1}{\rho_{\frac{1}{2}}}\varepsilon_1\Psi_1-\left(\frac{1}{\rho_{\frac{1}{2}}}+\frac{1}{\rho_{-\frac{1}{2}}}\right)\varepsilon_0\Psi_0+\frac{1}{\rho_{-\frac{1}{2}}}\varepsilon_{-1}\Psi_{-1}\right]\\&=\frac{1}{\left(k_0\Delta\mathrm{z}\right)^2}\left[\rho_+\varepsilon_1\Psi_1-\rho_0\varepsilon_0\Psi_0+\rho_-\varepsilon_{-1}\Psi_{-1}\right].\end{aligned} \tag{43}$$

III. NUMERICAL RESULTS

A. MONTEREY-MIAMI PARABOLIC EQUATION GRID SIZES

The discretization of the ocean environment is necessary and defined by the mesh size (Δr, Δz) [5]. The depth mesh, Δz, is used to determine the desired fast Fourier transform (FFT) size, defined by *nz*. The relation between Δz and *nz* is defined as $nz=2z_{max}/\Delta z$ in the SSF algorithm, where z_{max} is the maximum computational depth and 2 is the factor to account for the image ocean technique common in SSF models. The scaling factor, *rzfact*, is multiplied by the depth mesh to determine the range step size, Δr. We get a uniform grid size when *rzfact*=1, while the range step size becomes greater than the depth grid size when *rzfact*>1, or vice versa.

In this chapter, we first apply the density-smoothing approach and then the hybrid SSF/FD method by using different step sizes and depth meshes. In each case, we compare our computed transmission loss with a benchmark solution based on the results computed from the normal mode model, Couple07, by Richard Evans [13]. The comparison between solutions is based on both signal amplitude and the modulation structure in range (which depends on the phase of the solution). In many cases, the amplitude is found to agree well, but the phase structure shows disagreement with the benchmark solutions.

After the examination of these two methods, we present a comparison between the two to show the convergence, sensitivity, and other differences of the density-contrast interface. Finally, for completeness, we show the effect of including the higher order correction term.

For all calculations presented in this thesis, the environment was based on a scenario originally defined by Hursky [9]. This consists of a Pekeris waveguide of depth 300 m with a water column sound speed of 1500 m/s overlying a semi-infinite sediment half-space of sound speed 1700 m/s. Except for the initial test, in which both the water and sediment densities equal 1.0 g/cm^3, the sediment density is defined as 1.5 g/cm^3.

Attenuation in the sediment is defined as 0.5 dB/λ or 0.294 dB/m/kHz, while the water column is assumed to be lossless. Pressure calculations were made for a point source at depth 180 m transmitting a single frequency of 100 Hz. For comparison, a transmission loss trace for a receiver depth of 100 m was extracted out to 20 km range.

B. NO DENSITY DISCONTINUITY CASE

As has been stated, the SSF algorithm is known to be very accurate in the prediction of transmission loss in the absence of the density discontinuities. In this paper, we confirmed the consistency of the SSF algorithm with our benchmark Couple07 solution for such an environment. Figure 1 shows the comparison of these two solutions out to 20 km range. The agreement is found to be excellent.

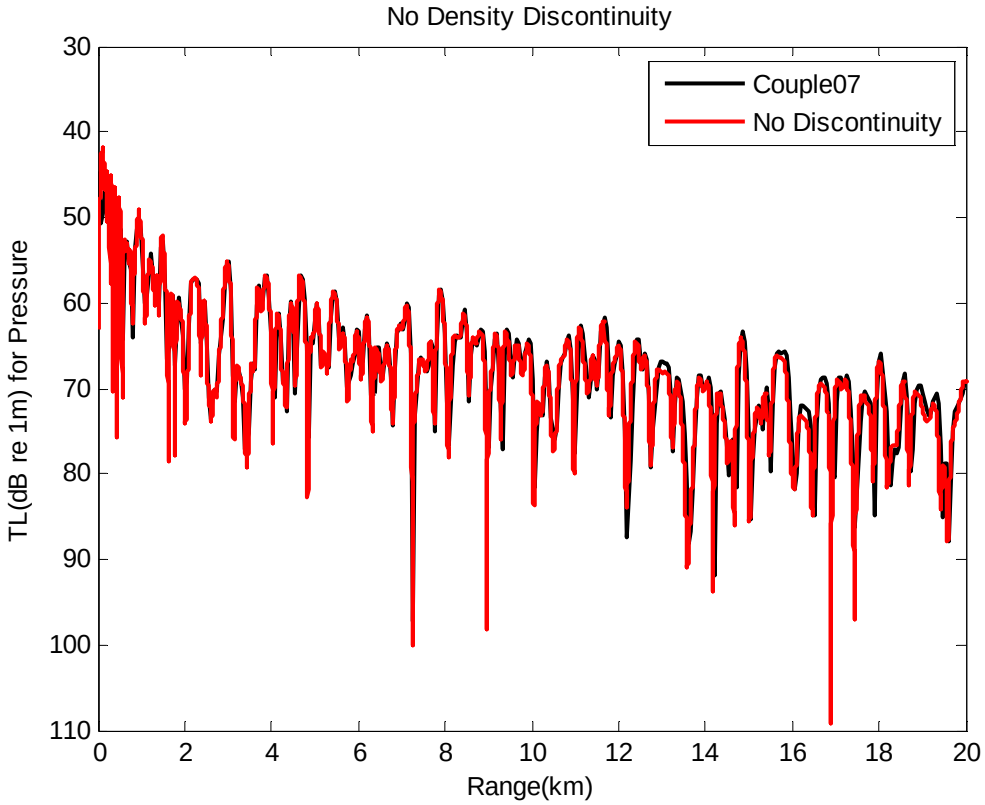

Figure 1. No Density Discontinuity vs. Couple07

C. DENSITY-SMOOTHING APPROACH

In the presence of density discontinuities across boundaries, the SSF algorithm utilizes the density-smoothing approach, as defined in the previous section. The mixing length, *L*, is a free variable that can be adjusted. In this work, we examined various mixing lengths: $1/4k_0$, $1/2k_0$, $1/k_0$, $3/2k_0$, $2/k_{0,}$ where k_0 is the reference wavenumber. The best results were obtained when *L* was set to $1/k_0$. We also tried different depth meshes, Δz, by adjusting *nz*, and range step sizes, Δr, by changing the scaling factor *rzfact*. We acquired an optimum stable, convergent solution with grid size $\Delta z=\lambda/15$ and *rzfact*=5, which corresponded to Δz=1 m with an FFT size of *nz*=4096, and range step size Δr=5 m, or $\lambda/3$. In order to see the effects of the depth mesh and range step size on the results using the density-smoothing approach, Figure 2 shows different *rzfact* values with fixed $\Delta z=\lambda/15$, and Figure 4 shows different Δz values with fixed *rzfact*=5. Each result is compared to our benchmark solution.

1. Δz=λ/15

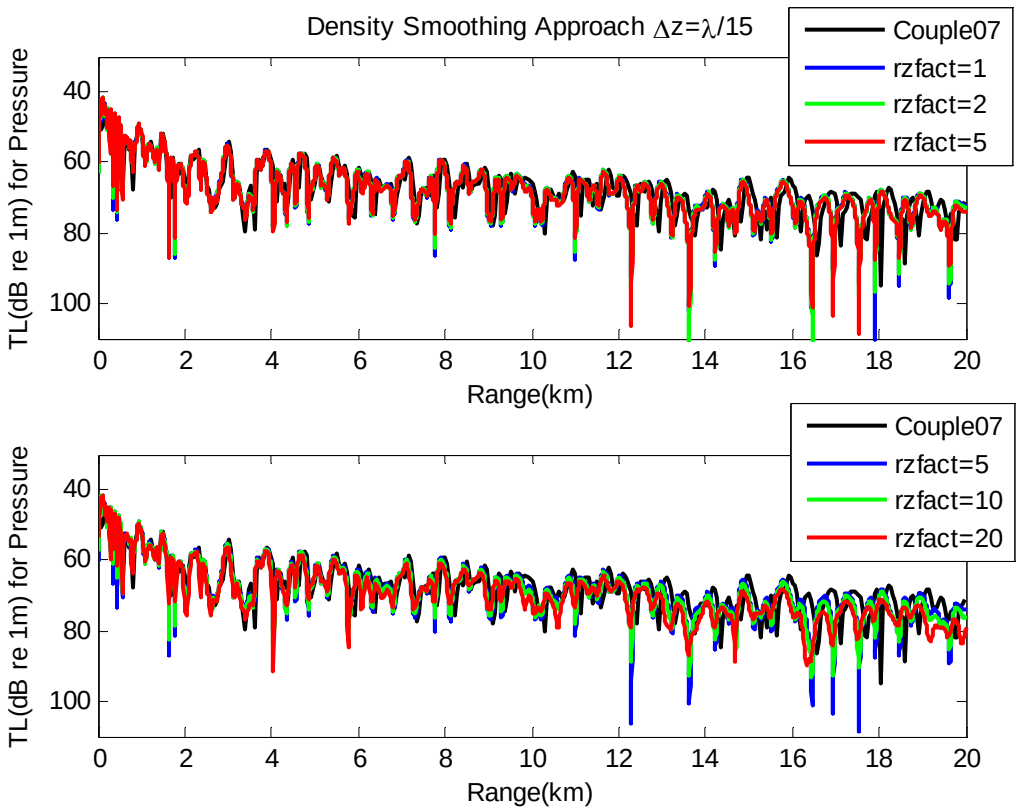

Figure 2. Density-Smoothing Approach, *rzfact*=1, 2, 5, 10, 20

Figure 2 shows the transmission loss comparisons with fixed value of $\Delta z = \lambda/15$. The scaling factor *rzfact* is chosen to be 1, 2, 5 in the first panel and 5, 10, 20 in the second panel. If we examine the plot, the smoothing approach matches the benchmark solution very well for the first several km for all *rzfact* values considered. However, between 4 and 10 km, a phase error appears and becomes significant, especially after 10 km. It is worth noting that, for $\Delta z \le \lambda/10$, convergence appears to occur for *rzfact*=5, with only very minor changes for smaller *rzfact* values.

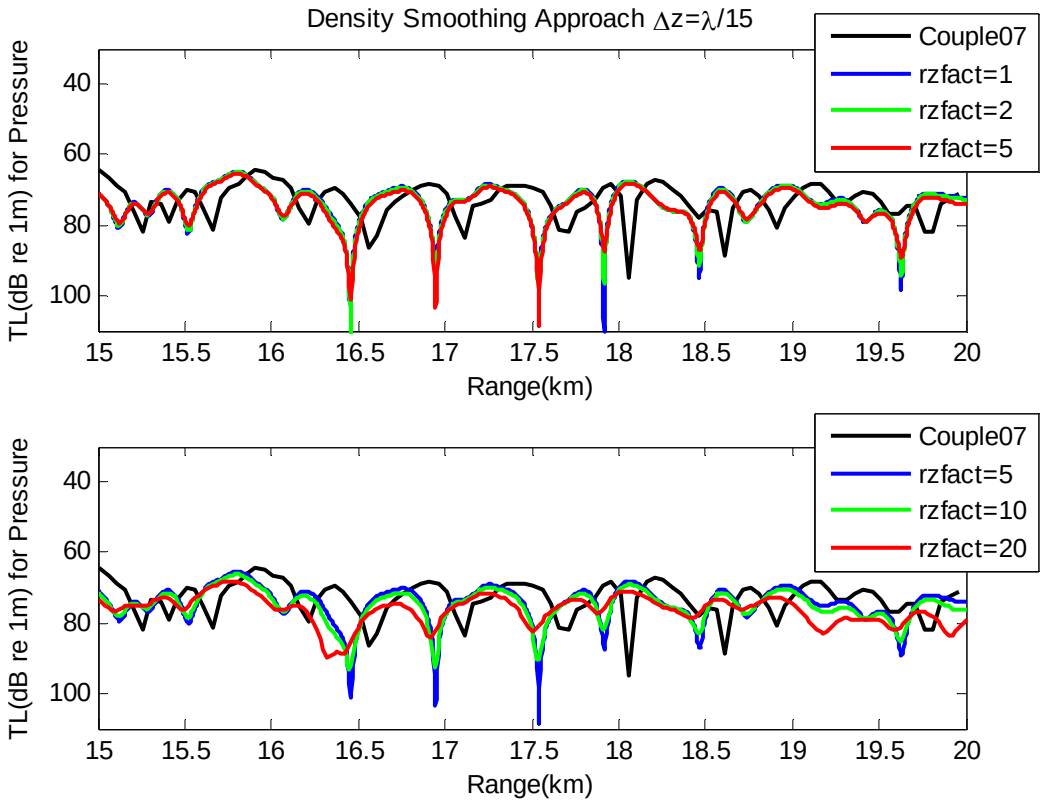

Figure 3. Convergence for *rzfact*=1, 2, 5, 10, 20

Figure 3 further illustrates the convergence of transmission loss results between 15 and 20 km. After examining different *rzfact* values, it is obvious that we cannot see a significant change for *rzfact*<5. However, when *rzfact*>5, the transmission loss amplitude changes slowly. For all cases, the phase error remains consistent and is unaffected by variations in *rzfact*.

2. rzfact=5

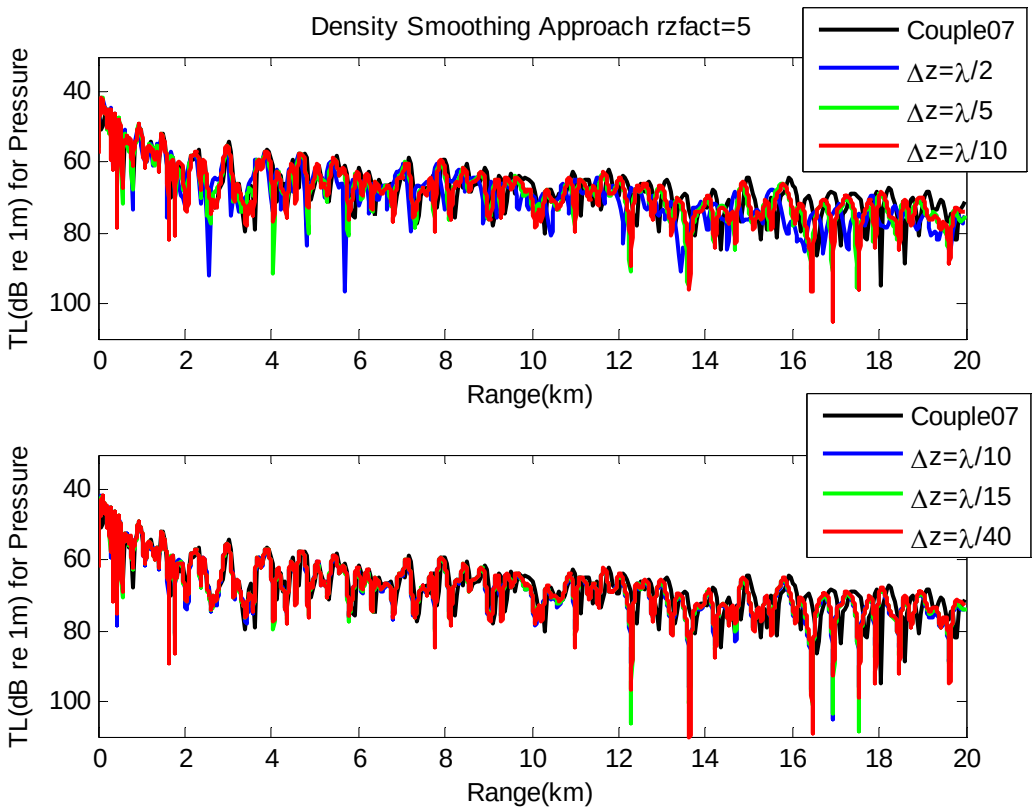

Figure 4. Density-Smoothing Approach, Δz=λ/2, λ/5, λ/10, λ/15, λ/40

Figure 4 shows different values of depth mesh, Δz, for a fixed value of *rzfact*=5. The solution converges for $\Delta z \le \lambda/10$, and $\Delta z = \lambda/15$ provides good agreement with the benchmark solution for the first several km. The solution begins to degrade at shorter ranges for $\Delta z \ge \lambda/5$, and when Δz<λ/2, the agreement is poor at all ranges. Even for the best solution, however, the phase error begins to appear at ranges beyond about 8 km.

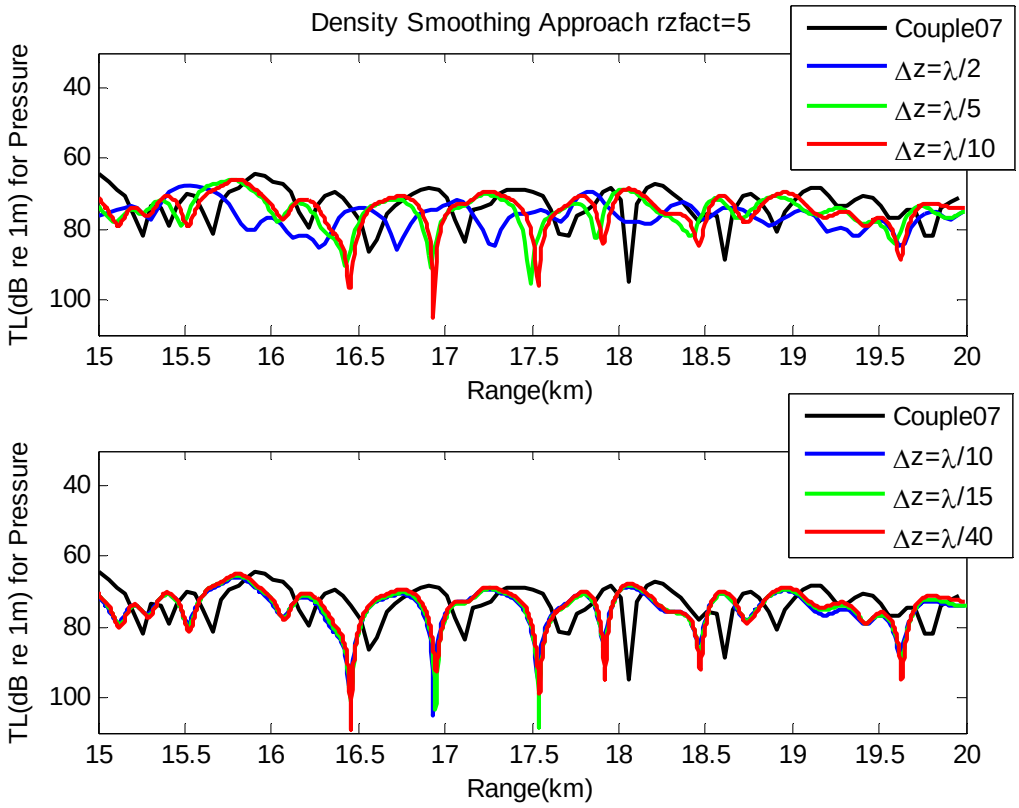

Figure 5. Convergence for $\Delta z=\lambda/2$, $\lambda/5$, $\lambda/10$, $\lambda/15$, $\lambda/40$

The expanded view in Figure 5 shows a stable behavior for $\Delta z<\lambda/5$. For these values, the amplitude stays constant, and we observe slight phase changes at ranges beyond 15 km. However, smaller values of Δz do not improve the phase match with the benchmark solution. In fact, for values of $\Delta z<\lambda/15$, numerical sensitivities begin to degrade the solution in the form of small-scale fluctuations in the result.

D. HYBRID SPLIT-STEP/FINITE DIFFERENCE ALGORITHM

For the hybrid SSF/FD approach, as with in the density-smoothing approach, we applied different range step sizes and depth meshes to find the optimum solution. Using the hybrid approach, we found improved agreement with our benchmark solution at longer ranges. We acquired the best result by applying a depth mesh $\Delta z=\lambda/15=1$ m, corresponding to an FFT size of *nz*=4096, and *rzfact*=10 or Δr=10 m.

1. Δz=λ/15

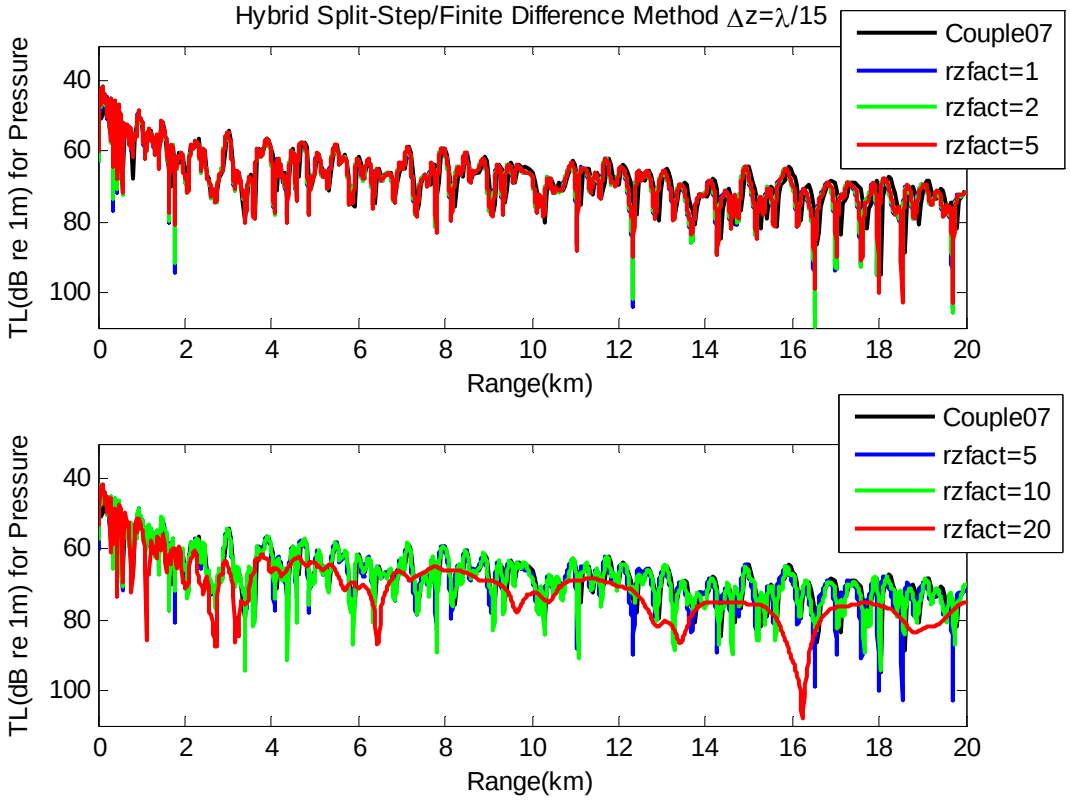

Figure 6. Hybrid Split-Step Method, *rzfact*=1, 2, 5, 10, 20

The first panel in Figure 6 shows the results for *rzfact*=1, 2, 5, and the second panel shows them for *rzfact*=5, 10, 20 with a fixed value of Δz=λ/15. It can be concluded from the plot that when *rzfact*≤5, then the transmission loss amplitude and phase error remain the same. The phase error begins to appear after 8 km but remains small for all *rzfact* values.

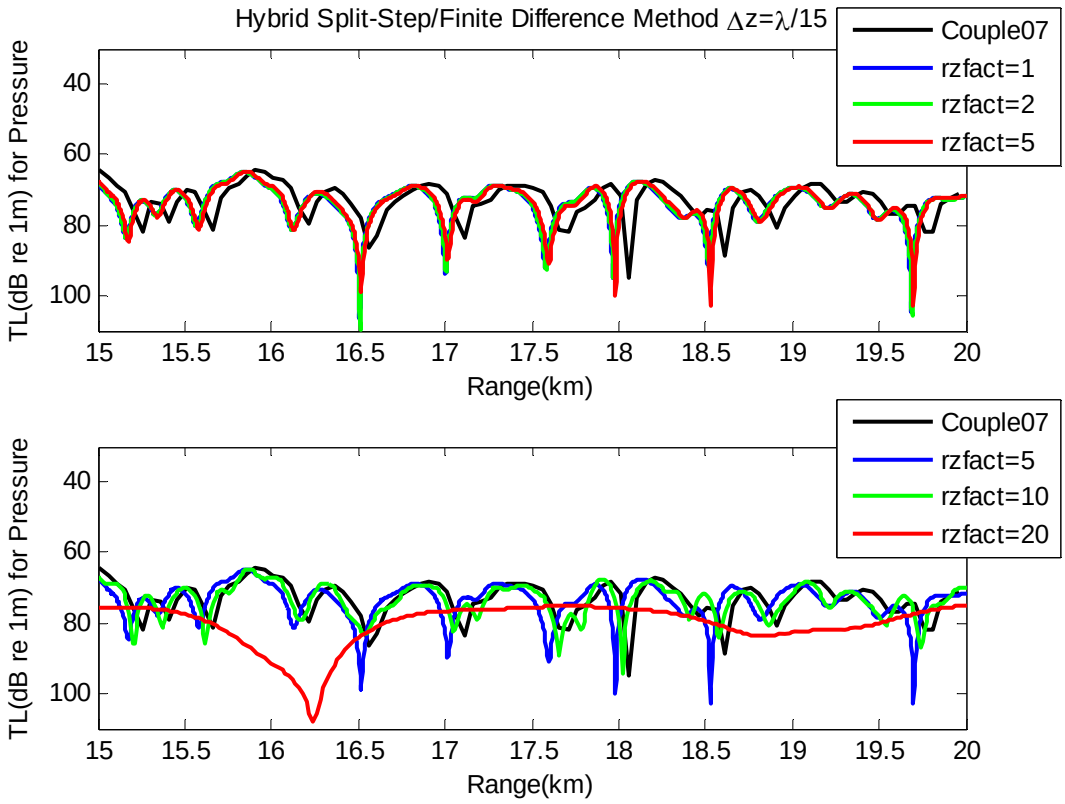

Figure 7. Convergence for *rzfact*=1, 2, 5, 10, 20

From the expanded view in Figure 7, an interesting observation is noted. First, as in the smoothing approach, the solution appears to converge to a stable result for *rzfact*≤5. However, in this case, a better match with the benchmark result is found just prior to convergence when *rzfact*=10. Larger values of *rzfact* give much worse results, so the improvement for *rzfact*=10 is likely just a coincidence. Therefore, the following results are computed for *rzfact*=5.

2. rzfact=5

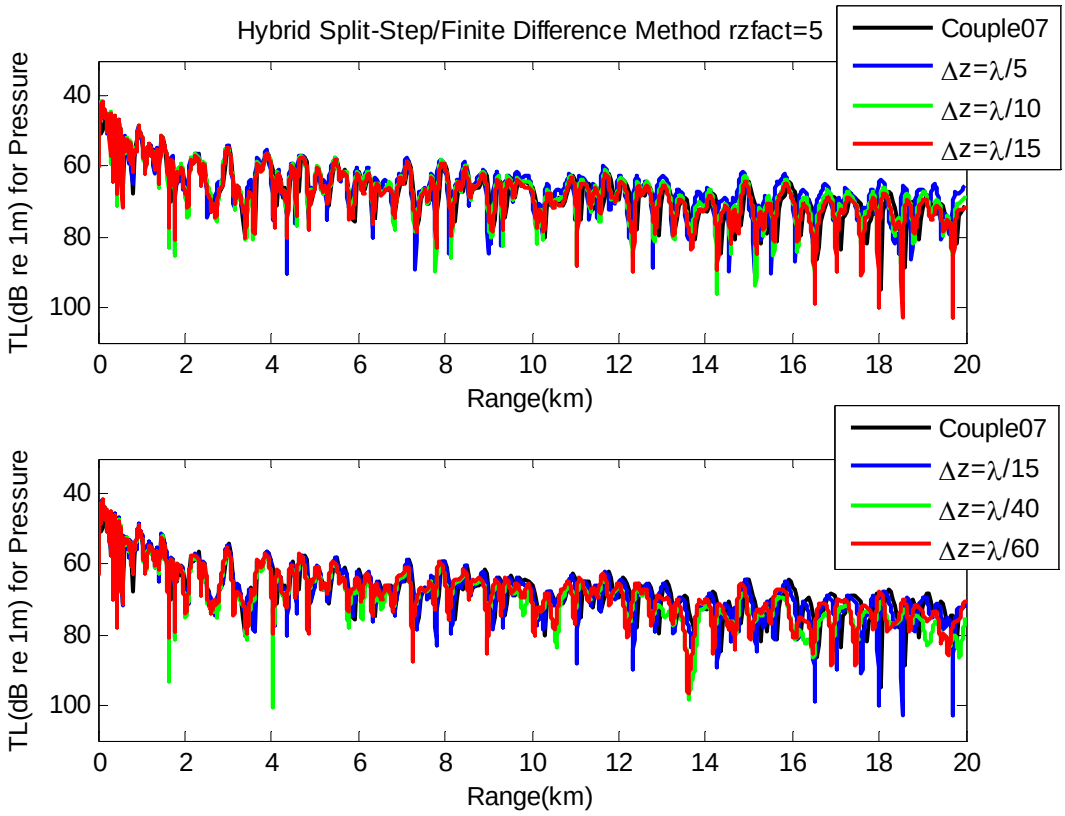

Figure 8. Hybrid Split-Step Method, Δz=λ/5, λ/10, λ/15, λ/40, λ/60

Figure 8 shows the various solutions at a fixed value of *rzfact*=5 for Δz= λ/15 to Δz= λ/60. It is obvious from the figure that decreasing the Δz values does not improve the result for *rzfact*=5 but introduces significant variability in the transmission loss amplitude. The results show the best match with Δz=λ/15, where agreement with the benchmark solution is good beyond 10 km. For $\Delta z \geq \lambda / 5$ (results computed but not shown), agreement degrades after a few kilometers, with very poor agreement at all ranges for $\Delta z \approx \lambda$.

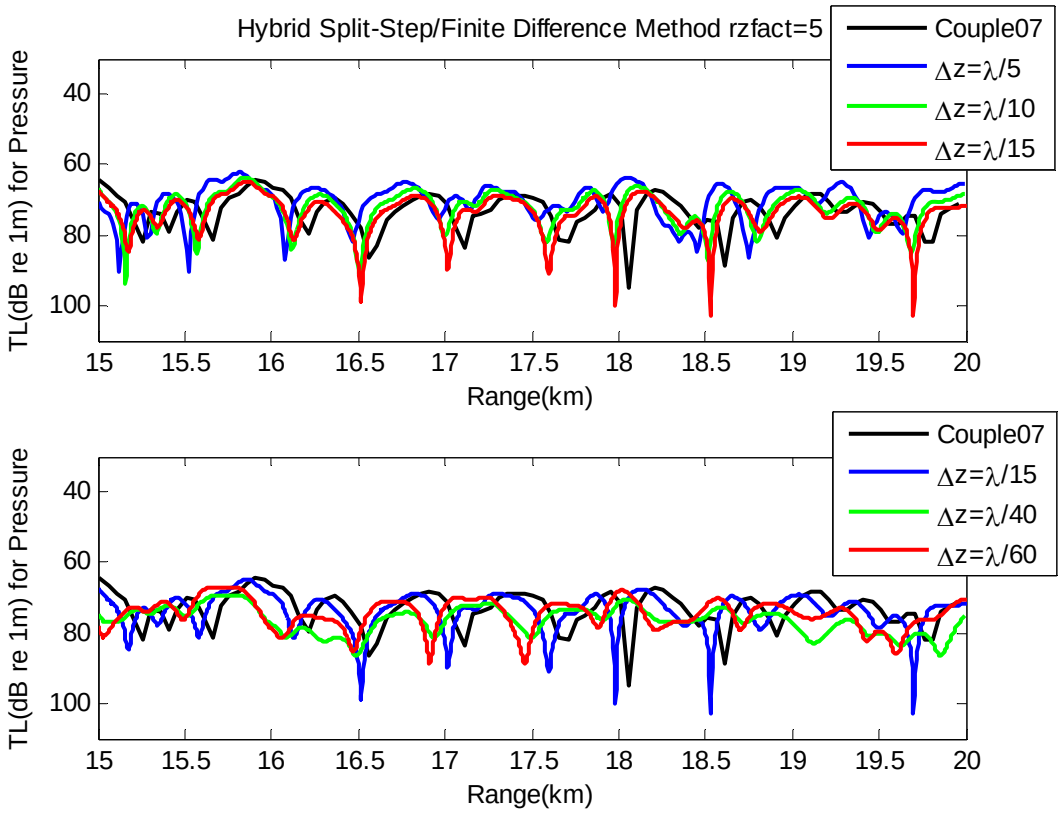

Figure 9. Convergence for $\Delta z=\lambda/5$, $\lambda/10$, $\lambda/15$, $\lambda/40$, $\lambda/60$

Figure 9 displays an expanded view of the last 5 km of the simulation as the Δz values decreased. The Δz values larger than $\lambda/15$ cause high phase errors and amplitude fluctuations, while we see good agreement with $\Delta z=\lambda/15$. It seems that the hybrid method is very sensitive to Δz values and show poor convergence in Δz.

E. COMPARISON OF DENSITY-SMOOTHING APPROACH AND HYBRID SPLIT STEP ALGORITHM

The comparison of the density-smoothing and hybrid split approaches gives unique results. Figure 10 shows the optimal solution of the two methods compared to benchmark solution Couple07. Both methods give the best result when $\Delta z=\lambda/15$ and converge when *rzfact*=5. The agreement with the benchmark is consistent out to about 8 km for the smoothing approach, while this number is almost 18 km for the hybrid method.

Both the smoothing approach and the hybrid method tend to converge when *rzfact* is around 5. For both methods, the results are stable when *rzfact*<5. In either case, it is recommended that *rzfact* should be between 2 and 5 in order to get accurate results. Figure 11 illustrates the last 5 km of the solution where hybrid method shows improved agreement with the benchmark solution. The transmission loss amplitudes of these two methods are almost the same, but the phase error of the smoothing approach is significantly higher than the hybrid method at these ranges.

One of the main differences between these two methods is their sensitivity to Δz, or nz. It can be observed from Figure 5 and Figure 9 that the hybrid method is more sensitive than the smoothing approach since it changes significantly by varying the Δz values and does not appear to reach a stable, convergent solution. So while the hybrid method appears to produce more accurate results, stability of this method appears to remain an issue.

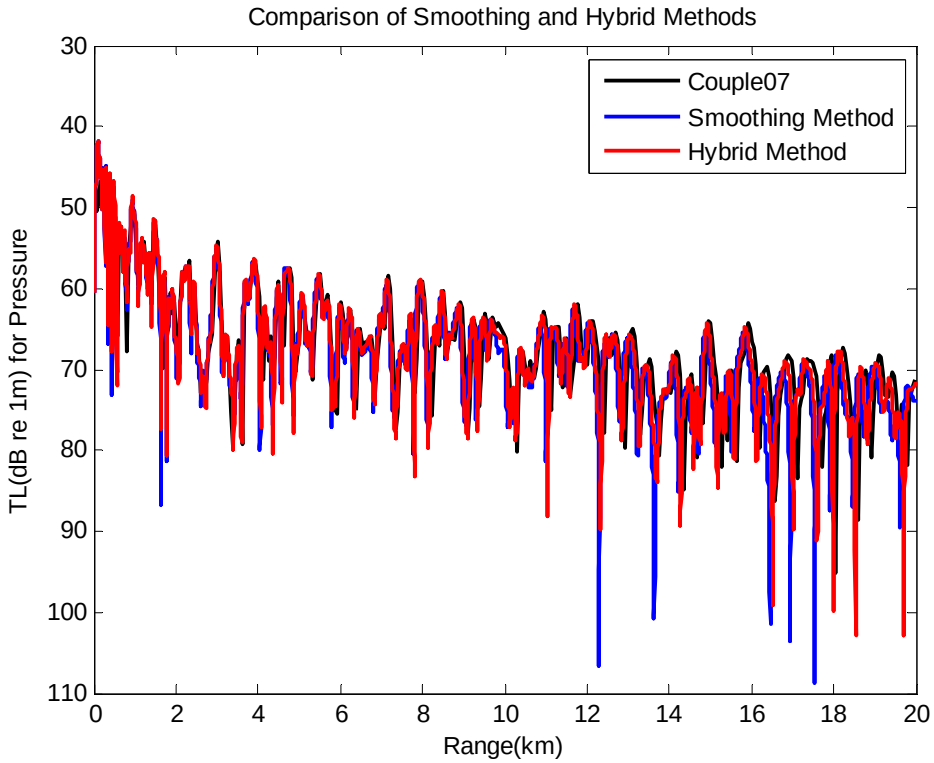

Figure 10. Smoothing and Hybrid Methods vs. Couple07 with $\Delta z=\lambda/15$ and $\Delta r=5*\Delta z=\lambda/3$

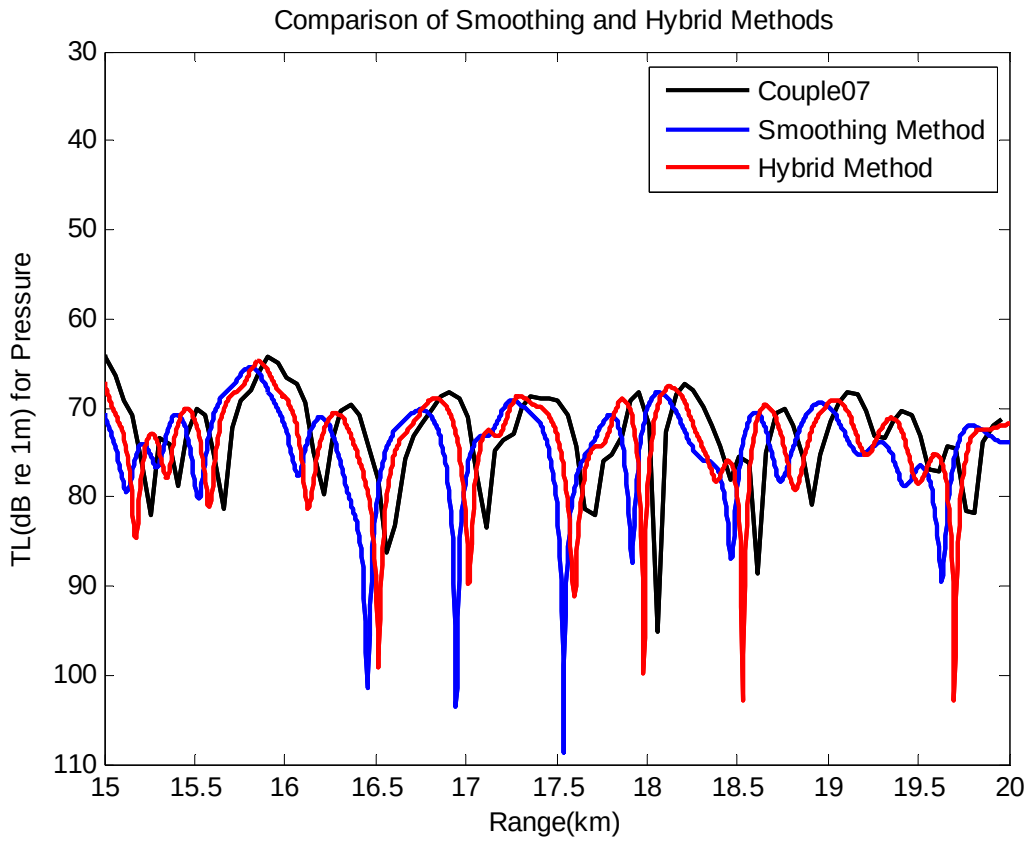

Figure 11. Convergence of Smoothing and Hybrid Methods with $\Delta z=\lambda/15$ and $\Delta r=5*\Delta z=\lambda/3$

F. COMPARISON OF HYBRID AND HYBRID HIGHER ORDER CORRECTION

Equations (15) and (36)–(43) define expressions that provide a higher order correction to the square root operator. In Figures 12 and 13, we see the comparison of the basic hybrid method and the hybrid higher order correction with the benchmark solution. For our case, we can conclude that higher order correction does not improve the solution any further.

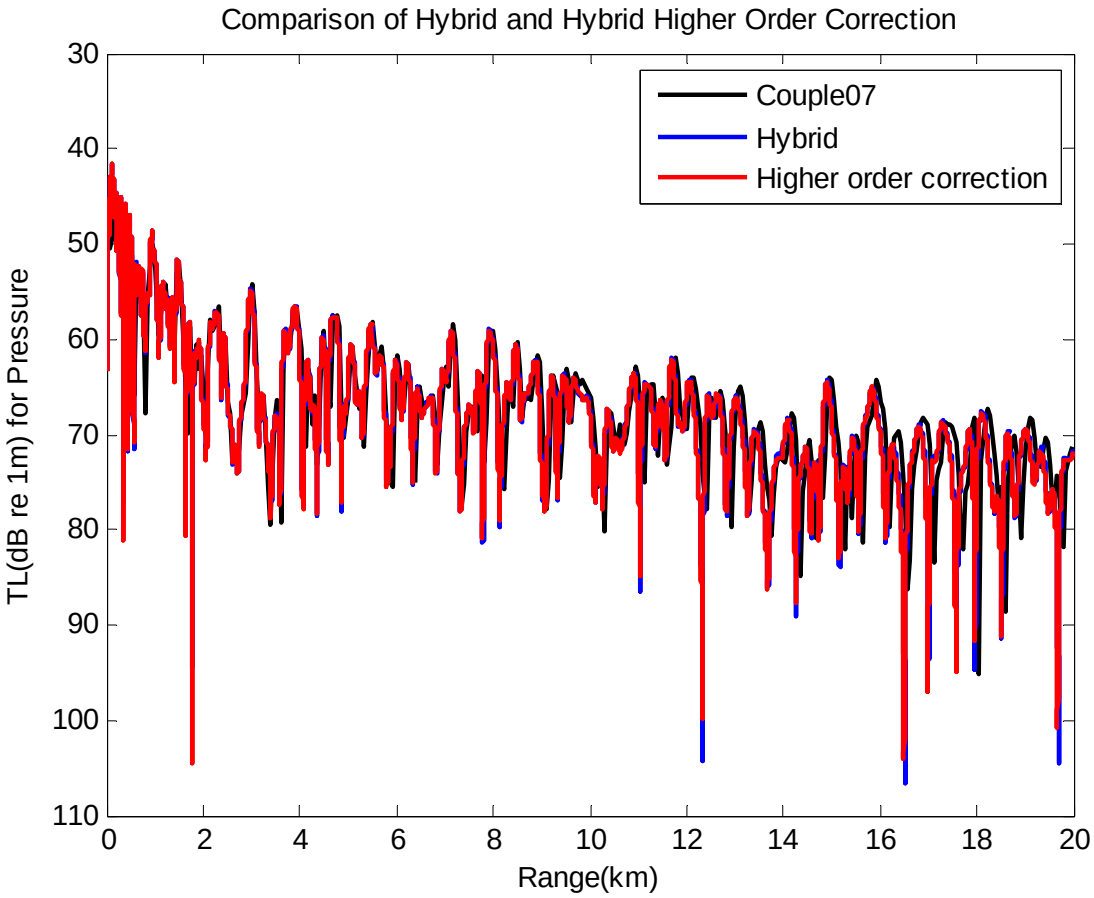

Figure 12. Comparison of Hybrid and Hybrid Higher Order Correction with $\Delta z=\lambda/15$ and $\Delta r=1*\Delta z=\lambda/15$

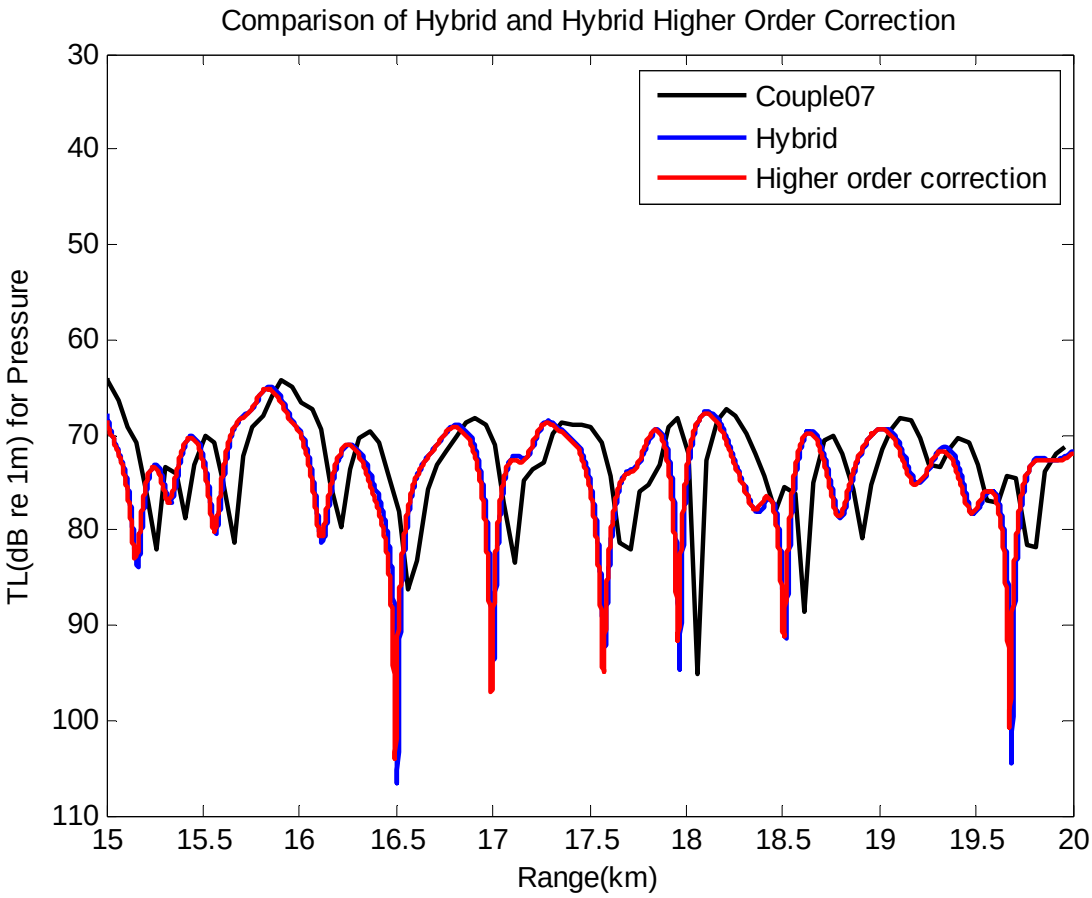

Figure 13. Comparison of Hybrid and Hybrid Higher Order Correction with $\Delta z=\lambda/15$ and $\Delta r=1*\Delta z=\lambda/15$

THIS PAGE INTENTIONALLY LEFT BLANK

IV. SUMMARY

The MMPE model, based on the SSF marching algorithm, has been used to predict the sound propagation in deep and shallow water environments for many years. Many studies have confirmed MMPE's accuracy in a wide variety of environments. However, in the presence of boundary density discontinuities, phase errors have been known to appear due to bottom interactions. This degrades the model's long-range accuracy. In this thesis, we compared results of the split-step density-smoothing and hybrid split-step/finite difference methods to treat the density discontinuity at the water-bottom interface. Of particular interest was the potential reduction in the phase errors using the hybrid approach, which could then be easily implemented into existing versions for the MMPE with the goal of improving the model's long range accuracy.

For the simple environment examined in this thesis, the SSF was found to give results consistent with a benchmark solution out to several kilometers, but beyond that, the phase errors accumulated and became significant after 10 km. In our examination, we obtained the optimum result by defining a depth mesh, $\Delta z=\lambda/15$. We also found that decreasing the depth mesh does not decrease the phase error significantly, and that the method tends to converge when Δz is between $\lambda/10$ and $\lambda/15$. Similarly, the range step size plays an important role in determining the best solution. The optimum result for that approach is obtained by a range step size $\Delta r=\lambda/3$, corresponding to scaling factor, *rzfact*=5.

The hybrid split-step/finite difference method resulted in improved solutions compared to our benchmark. This approach produced results that closely matched the benchmark results computed using Couple07. The best result was obtained with a depth mesh $\Delta z=\lambda/15$ and range step size $\Delta r=2\lambda/3$ corresponding to *rzfact*=10. However, convergence was achieved at *rzfact*=5. It is worth noting that both methods produced optimal results for the same mesh sizes.

For both methods, we found that for a fixed depth mesh of $\Delta z \approx \lambda/15$, the solution converged to a reasonably stable state for $\Delta r \le 5\Delta z = \lambda/3$. However, for a fixed

range step size of $\Delta r = \lambda/3$, only the split-step smoothing method appeared to converge to a stable state for decreasing values of Δz. The hybrid method appeared to reach an optimal solution at roughly the same depth mesh scale as the split-step smoothing method, $\Delta z \approx \lambda/15$, but appeared to degrade for much smaller values of Δz. This suggests that the finite difference approach to the density discontinuity is much more sensitive to the choice of Δz. While the solution is improved, this lack of stability should be treated with care. Future work should investigate the differences in sensitivity and convergence between these two methods in more detail.

Finally, we evaluated the influence of the higher order correction in the hybrid method. For this simple environment, it did not improve the solution significantly. Due to the added complexity of this correction and the lack of significant improvement, its inclusion in future updates of the MMPE model is not recommended.

APPENDIX. MATLAB CODES FOR HYBRID METHOD

This Matlab program performs a simple, range-independent calculation of a Pekeris waveguide problem as defined by Paul Hursky. The calculation is based on a split-step Fourier method which, when using the density-smoothing approach defined by Tappert and utilized in MMPE, shows phase errors that accumulate with range. In this code, the hybrid method of Yevick and Thomson is implemented in order to test the correction of the phase error by eliminating the smoothing approach.

```
%% PARAMETERS
format long
zbot=300; % bottom interface depth
D=4*zbot; % max computational depth of real ocean
zs=180;  % source depth
freq=100; % CW signal
cw=1500; % sound speed in the ocean
cb=1700; % sound speed in the bottom
c0=1500; % reference sound speed
lambda=c0/freq;  % reference wavelength
dz=lambda/10;   % first estimate of dz
NZ=round(2*D/dz); % first estimate of NZ
NZ=nextpow2(NZ); % round up to next power of 2 for FFT size
NZ=2.^NZ;
D=(NZ/2)*dz;   % max computational depth
z1=(1/2)*D;    % depth to begin spatial domain filtering
```

```
nb=floor(zbot/dz)+1; % depth index of bottom interface
rzfact=2;      % scaling factor between dr and dz (
dr=rzfact*dz;    % range step size
dkz=pi/D;                  % vertical wavenumber sampling
k0=(2*pi*freq)/c0;  % reference wavenumber
k1=(3/4)*k0;     % wavenumber to begin wavenumber domain filtering
R0=1;          % reference range
Rmax=20000;    % max computational range
NR=floor(Rmax/dr); % number of range steps in calculation
% Density Parameters
rho_w=1000; % density in water
rho_b=1500; % density in bottom
% %Preallocate arrays/matrices
kz=zeros(1,NZ);
x=zeros(1,NZ);
A=zeros(1,NZ);
B=zeros(1,NZ);
psi=zeros(1,NZ);
FK=ones(1,NZ);
Top=zeros(1,NZ);
PROPK=zeros(1,NZ);
z=zeros(1,NZ/2);
FZ=ones(1,NZ/2);
cz=zeros(1,NZ/2);
```

```
rho=zeros(1,NZ/2);
rho_m=zeros(1,NZ/2);
rho_t=zeros(1,NZ/2);
rho_p=zeros(1,NZ/2);
n_prime_sq=zeros(1,NZ/2);
atten=zeros(1,NZ/2);
atten_e=zeros(1,NZ/2);
Uop=zeros(1,NZ/2);
PROPZ=zeros(1,NZ/2);
press=zeros(NZ,NR);
r=zeros(1,NR);
TL=zeros(NZ,NR);
% Hybrid Method Parameters
se=(k0*dz).^2;
delta=k0*dr;
alpha=(1/4)*(1-1i*delta);
beta=(1/4)*(1+1i*delta);
q1=(rho_w-rho_b)/(3*rho_w+rho_b);
q2=(rho_b-rho_w)/(3*rho_b+rho_w);
q3=(rho_w-rho_b)/(rho_w+3*rho_b);
q4=(rho_b-rho_w)/(rho_b+3*rho_w);
a1=(1-(alpha/se)*q1);
a2=(alpha/se)*q1;
a3=(alpha/se)*q4;
```

```
a4=(1-(alpha/se)*(q3+q4));

a5=(alpha/se)*q3;

a6=(alpha/se)*q2;

a7=(1-(alpha/se)*q2);

b1=(1-(beta/se)*q1);

b2=(beta/se)*q1;

b3=(beta/se)*q4;

b4=(1-(beta/se)*(q3+q4));

b5=(beta/se)*q3;

b6=(beta/se)*q2;

b7=(1-(beta/se)*q2);

 % factors used in algebraic solution of tridiagonal matrix

fact0=1./(a4-a2*a3/a1-a5*a6/a7);

fact1=(b3-b1*a3/a1)*fact0;

fact2=(b4-b2*a3/a1-b6*a5/a7)*fact0;

fact3=(b5-b7*a5/a7)*fact0;

% produce r=0 in kz-domain

kz=[-NZ/2:(NZ/2-1)]*dkz;

x=kz/k0;

A=(1-x.^2).^(-1/4);

B=-1i*NZ*dkz*sqrt(2/(pi*k0))*sin(kz*zs);

psi=A.*B;
```

```
% Wavenumber domain filter
for ii=1:NZ;
 if -k0<kz(ii) && kz(ii)<-k1 ;
    FK(ii)=(cos((2*pi/k0)*(kz(ii)-k1))).^2;
 elseif k1<kz(ii) && kz(ii)<k0;
    FK(ii)=(cos((2*pi/k0)*(kz(ii)-k1))).^2;
 elseif kz(ii)<-k0;
    FK(ii)=0;
 elseif k0<kz(ii);
    FK(ii)=0;
 end
end
FK=fftshift(FK);
psi=fftshift(psi).*FK; % starting field with wavenumber filter applied in FFT order
psi=ifft(psi); % transform to z-domain
% Diffraction propagator (kz-domain)
Top=1-sqrt(1-x.^2);
PROPK=exp(-1i*k0*dr*Top);
PROPK=fftshift(PROPK); % put in FFT order for application in SSF algorithm
% Depth
z=[0:NZ/2-1]*dz;
for IZ=1:NZ/2;
 if 0<=z(IZ) && z(IZ)<=z1;
```

```
    FZ(IZ)=1;
   elseif z1<z(IZ) && z(IZ)<=(D-dz);
    FZ(IZ)=(cos((pi/(2*(D-z1)))*(z(IZ)-z1))).^2;
   end
  end
  % Sound Speed Profile (real ocean part of z-domain)
  cz=size(z);
  cz(1:nb-1)=cw;
  cz(nb)=0.5*(cw+cb);
  cz(nb+1:NZ/2)=cb;
  n_prime_sq=(c0./cz).^2; % For density smoothing approach use effective index of refraction instead
  % Density Profile (real ocean part of z-domain)
  rho=size(z);
  rho(1:nb-1)=rho_w;
  rho(nb)=0.5*(rho_w+rho_b);
  rho(nb+1:NZ/2)=rho_b;
  % Bottom attenuation
  atten(nb)=0.5*(0.5); % in dB/lambda - applying Heaviside step function intermediate value
  atten(nb+1:NZ/2)=0.5; % in dB/lambda
  atten_e=atten.*(freq./cz)/8.686; % in 1/m
  % Lens propagator (real ocean part of z-domain)
  Uop=(1-sqrt(n_prime_sq));
```

```
PROPZ=exp(-1i*k0*dr*Uop).*exp(-atten_e*dr);
% Range increament
for IR=1:NR;
  psi(1:NZ/2)=PROPZ.*psi(1:NZ/2); % lens propagator to real ocean
  psi(1:NZ/2)=FZ.*psi(1:NZ/2);   % z-domain filter to real ocean
  psi(NZ/2+2:NZ)=-psi(NZ/2:-1:2); psi(NZ/2+1)=0; % odd symmetry
  psi=fft(psi);  % transform to kz-domain - output in FFT order
  psi=psi.*PROPK; % diffraction propagator
  psi=psi.*FK;  % kz-domain filter
  psi=ifft(psi); % transform to z-domain - output in FFT order
   % Hybrid method - apply in real ocean only (odd symmetry applied after lens
propagator)
  if IR==1
   disp('Using hybrid finite difference method for density')
  end
  tmp=fact1*psi(nb-1)+fact2*psi(nb)+fact3*psi(nb+1);
  psi(nb-1)=b1/a1*psi(nb-1)+b2/a1*psi(nb)-a2/a1*tmp;
  psi(nb+1)=b6/a7*psi(nb)+b7/a7*psi(nb+1)-a6/a7*tmp;
  psi(nb)=tmp;
% Compute Pressure Field
  r(IR)=IR*dr;
  press(:,IR)=psi*sqrt(R0/r(IR)); % store pressure field in FFT order
end
```

```
% Transmission Loss
TL=-20*log10(abs(press(1:NZ/2,:)));
zout=100;
nout=find(z>=zout, 1 );
if (zout-z(nout-1))<(z(nout)-zout)
  nout=nout-1;
end
figure
plot(r/1000,TL(nout,:),'r');axis ij;
xlim ([0 20])
ylim ([30 110])
hold on
plot(rng,tlz,'k');axis ij;
xlim ([0 20])
ylim ([30 110])
legend('PE-SSF-YT-1stOrder','Couple07')
title(['dr=' num2str(dr) 'm, lambda/dz=' num2str(lambda/dz) ', c0=' num2str(c0)
'm/s, rhob=' num2str(rho_b) 'kg/m^3'])
```

LIST OF REFERENCES

[1] F. B. Jensen, W. A. Kuperman, M. B. Porter, and H. Schmidt, *Computational Ocean Acoustics*, Woodbury, NY: AIP Press, 1993, pp. 343–405.

[2] F. D. Tappert, "The parabolic approximation method in underwater acoustics," *J. Acoust. Soc. Am.*, vol. 55, no. S1, pp. S34, Apr. 1974.

[3] R. H. Hardin and F. D. Tappert, "Applications of the split-step Fourier method to the numerical solution of nonlinear and variable coefficient wave equations," *SIAM*, vol. 15, no. 2, pp. 423, Apr. 1973.

[4] D. J. Thomson and N. R. Chapman, "A wide-angle split-step algorithm for the parabolic equation," *J. Acoust. Soc. Am.*, vol. 74, no. 6, pp. 1848–1854, Dec. 1983.

[5] K. B. Smith, "Convergence, stability, and variability of shallow water acoustic predictions using a split-step Fourier parabolic equation model," *J. Compıt. Acous.*, vol. 9, no. 1, pp. 243–285, Apr. 2001.

[6] M. D. Feit and J. A. Fleck, Jr., "Light propagation in graded-index fibers," *Applied Optics*, vol. 17, no. 24, pp. 3990–3998, Dec. 1978.

[7] D. Yevick and D. J. Thomson, "A hybrid split-step/finite-difference PE algorithm for variable-density media," *J. Acoust. Soc. Am.*, vol. 101, no. 3, pp. 1328–1335, Mar. 1997.

[8] M. D. Owens, "Comparison of different implementation options for density discontinuity in split step Fourier parabolic equation models," M.S. thesis, Physics Dept., Naval Postgraduate School, Monterey, CA, 2014.

[9] K. B. Smith and P. Hursky, private communication, 2013.

[10] K. B. Smith, D. J. Thomson, and P. Hursky, "An investigation into the bottom interface treatment in parabolic equation models utilizing split-step Fourier and finite-difference algorithms," *J. Acoust. Soc. Am.*, vol. 135, p. 2430, 2014.

[11] K. B. Smith, "A synopsis of the hybrid method for bottom density discontinuity," unpublished.

[12] D. J. Thomson, "Wide-angle parabolic equation solutions to two range-dependent benchmark problems," *J. Acoust. Soc. Am.*, vol. 87, no. 4, pp. 1514–1520, 1990.

[13] R. B. Evans, "A coupled mode solution for acoustic propagation in a waveguide with stepwise depth variations of a penetrable bottom," *J. Acoust. Soc. Am.*, vol. 74, no. 1, pp. 188–195, 1983.

THIS PAGE INTENTIONALLY LEFT BLANK

INITIAL DISTRIBUTION LIST

1. Defense Technical Information Center
   Ft. Belvoir, Virginia

2. Dudley Knox Library
   Naval Postgraduate School
   Monterey, California